Supplementary Information

Self-assembly of Freely-rotating Polydisperse Cuboids: Unveiling the Boundaries of the Biaxial Nematic Phase

Effran Mirzad Rafael,[1] Daniel Corbett,[1] Alejandro Cuetos,[2] and Alessandro Patti[1]

[1]*Department of Chemical Engineering and Analytical Science, The University of Manchester, Manchester, M13 9PL, United Kingdom*
[2]*Department of Physical, Chemical and Natural Systems, Pablo de Olavide University, 41013 Sevilla, Spain*

I. ORDER PARAMETERS

The classification of our equilibrium phases was done by examining orientational and positional ordering. To measure the long-range orientational order, we diagonalised the following second-rank symmetric tensor:

$$\mathbf{Q}^{\lambda\lambda} = \frac{1}{2N_p}\left\langle \sum_{i=1}^{N_p} \left(3\hat{\lambda}_i \cdot \hat{\lambda}_i - \mathbf{I}\right) \right\rangle \tag{1}$$

where i indicates a generic particle, $\hat{\lambda} = \hat{x}, \hat{y}, \hat{z}$ denotes its unit orientation vector along its length (L), width (W) and thickness (T), respectively, $\mathbf{I}$ is the second-rank unit tensor, and the angular brackets denote ensemble average. When diagonalised, the tensor $\mathbf{Q}^{\lambda\lambda}$ produces three eigenvalues $S_{2,L}, S_{2,W}$, and $S_{2,T}$ and their corresponding eigevectors $\hat{\mathbf{n}}, \hat{\mathbf{m}}$, and $\hat{\mathbf{l}}$. For example, the tensor $\mathbf{Q}^{zz}$ is related to the largest eigenvalue $S_{2,L}$, and corresponding eigenvector $\hat{\mathbf{n}}$, which provides alignment along the particle axis $\hat{x}$. The calculation of the eigenvalues $S_{2,L}$, $S_{2,W}$ and $S_{2,T}$, referred to as uniaxial order parameters, allows to distinguish between an isotropic phase, where all eigenvalues vanish, and an ordered phase, where at least one of the eigenvalues is significantly larger than zero. We arbitrarily set the formation of a uniaxial LC phase when one of the three uniaxial order parameters is at least 0.40 (see Table I). To assess the system biaxiality, the biaxial order parameter for each axes can be calculated using the same symmetric tensor. To this end, the following equation is applied:

$$B_{2,L} = \frac{1}{3}\left(\hat{\mathbf{m}} \cdot \mathbf{Q}^{xx} \cdot \hat{\mathbf{m}} + \hat{\mathbf{l}} \cdot \mathbf{Q}^{yy} \cdot \hat{\mathbf{l}} - \hat{\mathbf{m}} \cdot \mathbf{Q}^{yy} \cdot \hat{\mathbf{m}} - \hat{\mathbf{l}} \cdot \mathbf{Q}^{xx} \cdot \hat{\mathbf{l}}\right) \tag{2}$$

The other two biaxial order parameters, $B_{2,W}$ and $B_{2,T}$, can be calculated from similar expressions. To determine B_2, it is sufficient to monitor the fluctuations of axes perpendicular to the main nematic director. For instance, if $S_{2,L}$ is the dominant uniaxial order parameter, it is sufficient to monitor $B_{2,L}$ as it indicates the fluctuations along axes $\hat{y}$ and $\hat{z}$ in the planes of $\hat{\mathbf{m}}$ and $\hat{\mathbf{l}}$. Table I shows the criteria to determine the symmetry of the phases observed in this work and consistent with Ref [1]. In Tables II to VIII, we report the uniaxial and biaxial order parameters of HBPs with $\sigma_L = 0.05$ to $\sigma_L = 0.30$.

TABLE I: Criteria of uniaxial and biaxial order parameters used in the classification of HBPs.

$S_{2,L}$	$S_{2,T}$	$S_{2,W}$	$B_{2,L}$ or $B_{2,T}$	Phase
0.00 - 0.20	0.00 - 0.20	0.00 - 0.20	-	Isotropic
0.40 - 1.00	0.00 - 0.35	0.00 - 0.35	0.00 - 0.30	Uniaxial prolate
0.00 - 0.35	0.40 - 1.00	0.00 - 0.35	0.00 - 0.30	Uniaxial oblate
0.40 - 1.00	0.35 - 1.00	0.35 - 1.00	0.20 - 0.35	Weak biaxial prolate
0.35 - 1.00	0.40 - 1.00	0.35 - 1.00	0.20 - 0.35	Weak biaxial oblate
0.40 - 1.00	0.40 - 1.00	0.40 - 1.00	0.35 - 1.00	Biaxial

TABLE II: Reduced pressure, packing fraction, uniaxial and biaxial order parameters for HBPs of $\sigma_L = 0.05$. Absolute errors are less than 5×10^{-3}.

Phase	P^*	η	$S_{2,T}$	$S_{2,W}$	$S_{2,L}$	B_2
I	0.060	0.265	0.039	0.019	0.032	0.012
I	0.070	0.286	0.057	0.021	0.061	0.021
I	0.075	0.297	0.086	0.023	0.073	0.025
N_U^-	0.080	0.310	0.402	0.070	0.195	0.026
N_U^+	0.085	0.326	0.257	0.131	0.577	0.037
N_U^+	0.090	0.344	0.264	0.164	0.726	0.043
N_U^+	0.095	0.375	0.265	0.247	0.894	0.042
Sm_U^+	0.100	0.391	0.239	0.233	0.912	0.009
Sm_U^+	0.110	0.415	0.261	0.256	0.926	0.035
Sm_U^+	0.120	0.437	0.248	0.233	0.931	0.009
Sm_U^+	0.130	0.458	0.261	0.233	0.921	0.011
Sm_U^+	0.140	0.477	0.275	0.245	0.931	0.018
Sm_U^+	0.160	0.513	0.312	0.243	0.907	0.068
Sm_U^+	0.180	0.546	0.307	0.243	0.915	0.053
Sm_B^+	0.200	0.573	0.431	0.331	0.888	0.208

TABLE III: Reduced pressure, packing fraction, uniaxial and biaxial order parameters for HBPs of $\sigma_L = 0.10$. Absolute errors are less than 5×10^{-3}.

Phase	P^*	η	$S_{2,T}$	$S_{2,W}$	$S_{2,L}$	B_2
I	0.060	0.265	0.052	0.019	0.052	0.024
I	0.070	0.288	0.081	0.024	0.068	0.023
I	0.075	0.297	0.114	0.024	0.090	0.027
N_U^-	0.080	0.314	0.595	0.109	0.218	0.007
N_U^+	0.090	0.342	0.231	0.160	0.752	0.004
N_U^+	0.100	0.373	0.271	0.238	0.863	0.039
Sm_U^+	0.105	0.395	0.260	0.249	0.921	0.022
Sm_U^+	0.110	0.410	0.248	0.246	0.923	0.016
Sm_U^+	0.120	0.429	0.249	0.249	0.940	0.018
Sm_U^+	0.130	0.449	0.251	0.243	0.923	0.015
Sm_U^+	0.140	0.478	0.265	0.243	0.940	0.019
Sm_U^+	0.160	0.507	0.398	0.328	0.901	0.180
Sm_B^+	0.180	0.539	0.455	0.385	0.913	0.223
Sm_B^+	0.200	0.564	0.562	0.474	0.893	0.387

TABLE IV: Reduced pressure, packing fraction, uniaxial and biaxial order parameters for HBPs of $\sigma_L = 0.15$. Absolute errors are less than 5×10^{-3}.

Phase	P^*	η	$S_{2,T}$	$S_{2,W}$	$S_{2,L}$	B_2
I	0.060	0.268	0.053	0.026	0.048	0.016
I	0.070	0.292	0.269	0.051	0.184	0.048
N_U^-	0.078	0.310	0.490	0.115	0.261	0.070
N_U^-	0.080	0.319	0.602	0.148	0.282	0.080
N_U^-	0.090	0.343	0.757	0.183	0.261	0.024
N_U^+	0.100	0.371	0.290	0.231	0.830	0.044
N_U^+	0.110	0.398	0.260	0.209	0.840	0.032
Sm_U^+	0.120	0.421	0.357	0.283	0.848	0.111
Sm_U^+	0.130	0.445	0.384	0.284	0.833	0.151
Sm_U^+	0.140	0.465	0.405	0.293	0.824	0.183
Sm_U^+	0.150	0.484	0.389	0.287	0.843	0.156
Sm_B^+	0.160	0.503	0.557	0.434	0.843	0.360
Sm_B^+	0.180	0.540	0.672	0.566	0.866	0.536

TABLE V: Reduced pressure, packing fraction, uniaxial and biaxial order parameters for HBPs of $\sigma_L = 0.18$. Absolute errors are less than 5×10^{-3}.

Phase	P^*	η	$S_{2,T}$	$S_{2,W}$	$S_{2,L}$	B_2
I	0.060	0.266	0.061	0.024	0.058	0.024
I	0.070	0.289	0.259	0.051	0.182	0.039
N_U^-	0.078	0.305	0.515	0.124	0.263	0.064
N_U^-	0.080	0.314	0.642	0.131	0.219	0.018
N_U^+	0.090	0.341	0.258	0.174	0.723	0.029
N_U^+	0.100	0.362	0.258	0.205	0.812	0.032
N_U^+	0.110	0.387	0.281	0.233	0.861	0.037
N_U^+	0.120	0.411	0.413	0.316	0.840	0.113
N_B^+	0.130	0.433	0.491	0.375	0.837	0.295
N_B	0.140	0.455	0.641	0.498	0.822	0.465
N_B	0.150	0.481	0.670	0.520	0.825	0.485
Sm_B^-	0.160	0.496	0.910	0.588	0.667	0.521
Sm_B^-	0.180	0.546	0.955	0.647	0.683	0.552
Sm_B^-	0.200	0.573	0.948	0.646	0.692	0.567

TABLE VI: Reduced pressure, packing fraction, uniaxial and biaxial order parameters for HBPs of $\sigma_L = 0.20$. Absolute errors are less than 5×10^{-3}.

Phase	P^*	η	$S_{2,T}$	$S_{2,W}$	$S_{2,L}$	B_2
I	0.040	0.225	0.045	0.023	0.037	0.018
I	0.050	0.249	0.054	0.023	0.039	0.013
I	0.060	0.271	0.072	0.026	0.067	0.017
I	0.063	0.280	0.091	0.027	0.045	0.037
I	0.065	0.284	0.157	0.022	0.108	0.049
N_U^-	0.070	0.297	0.402	0.067	0.186	0.027
N_U^+	0.080	0.321	0.314	0.162	0.564	0.079
N_U^+	0.090	0.348	0.286	0.196	0.714	0.047
N_U^+	0.100	0.371	0.304	0.226	0.774	0.094
N_U^+	0.105	0.384	0.364	0.269	0.772	0.131
N_B	0.110	0.400	0.558	0.362	0.701	0.372
N_B	0.120	0.419	0.584	0.376	0.720	0.395
N_B	0.130	0.441	0.592	0.408	0.751	0.417
N_B	0.140	0.465	0.643	0.517	0.813	0.459
N_B	0.150	0.486	0.658	0.523	0.808	0.517
N_B	0.160	0.505	0.709	0.569	0.816	0.579
N_B	0.180	0.542	0.727	0.553	0.798	0.566
Sm_B^-	0.200	0.575	0.792	0.608	0.796	0.668

TABLE VII: Reduced pressure, packing fraction, uniaxial and biaxial order parameters for HBPs of $\sigma_L = 0.25$. Absolute errors are less than 5×10^{-3}.

Phase	P^*	η	$S_{2,T}$	$S_{2,W}$	$S_{2,L}$	B_2
I	0.040	0.226	0.044	0.021	0.040	0.017
I	0.050	0.249	0.055	0.026	0.050	0.020
I	0.060	0.276	0.086	0.030	0.106	0.027
I	0.063	0.281	0.124	0.030	0.120	0.041
I	0.065	0.285	0.122	0.029	0.140	0.047
N_U^-	0.070	0.300	0.457	0.109	0.201	0.030
N_U^-	0.075	0.314	0.581	0.129	0.223	0.037
N_U^-	0.080	0.324	0.592	0.143	0.269	0.072
N_U^-	0.090	0.350	0.750	0.203	0.278	0.065
N_U^-	0.095	0.361	0.787	0.200	0.260	0.042
N_B^+	0.100	0.374	0.548	0.344	0.654	0.222
N_B^+	0.110	0.398	0.616	0.386	0.663	0.301
N_B	0.120	0.423	0.635	0.423	0.687	0.443
N_B	0.130	0.446	0.690	0.540	0.780	0.457
N_B	0.140	0.463	0.664	0.510	0.788	0.518
N_B	0.160	0.507	0.671	0.508	0.783	0.524
N_B	0.180	0.542	0.682	0.498	0.767	0.530
N_B	0.200	0.570	0.718	0.541	0.783	0.574

TABLE VIII: Reduced pressure, packing fraction, uniaxial and biaxial order parameters for HBPs of $\sigma_L = 0.30$. Absolute errors are less than 5×10^{-3}.

Phase	P^*	η	$S_{2,T}$	$S_{2,W}$	$S_{2,L}$	B_2
I	0.040	0.227	0.047	0.021	0.052	0.021
I	0.050	0.253	0.088	0.026	0.076	0.021
I	0.060	0.280	0.154	0.028	0.180	0.041
N_U^-	0.068	0.300	0.466	0.010	0.202	0.031
N_U^-	0.070	0.304	0.515	0.125	0.229	0.051
N_U^-	0.080	0.328	0.629	0.115	0.263	0.055
N_U^-	0.090	0.355	0.733	0.182	0.255	0.046
N_U^-	0.095	0.366	0.727	0.209	0.306	0.054
N_B^+	0.100	0.381	0.684	0.365	0.545	0.359
N_B	0.110	0.402	0.633	0.418	0.674	0.467
N_B	0.120	0.426	0.719	0.497	0.692	0.477
N_B	0.130	0.450	0.704	0.542	0.768	0.561
N_B	0.140	0.467	0.727	0.571	0.779	0.603
N_B	0.160	0.509	0.748	0.587	0.785	0.609
N_B	0.180	0.548	0.827	0.658	0.806	0.684

II. PAIR CORRELATION FUNCTION

To distinguish nematic from smectic phases, we calculated the pair correlation function parallel to the nematic director(s), which formally reads:

$$g_{\parallel}(r_{\parallel}) = \frac{1}{N_p \rho S_{\parallel}} \left\langle \sum_i \sum_{j \neq i} \delta(r_{\parallel} - r_{\parallel,ij}) \right\rangle \tag{3}$$

where $\rho = N_p/V$, N_p is the number of particles, V the box volume, δ is the Dirac delta. $S_{\parallel}$ is a surface resulting from the intersection of a sphere with radius half of the simulation box and a plane perpendicular to the nematic director at a distance $r_{\parallel}$ from the center of the sphere. To practically evaluate $g_{\parallel}$ in our simulations, we employed the following expression [3]:

$$g_{\parallel}(r_{\parallel}) = \frac{1}{N_p \rho V_{\parallel}} \frac{N(r_{\parallel})}{N_c} \tag{4}$$

where N_c is the number of sampled configurations. $N(r_{\parallel})$ is the number of times that the distance between two particles projected along the nematic director, $r_{\parallel,ij}$, is in the interval $|r_{\parallel} + \Delta r_{\parallel}|$. Finally, $V_{\parallel}$ is the volume of this region, that can be calculated as

$$V_{\parallel} = \pi \left(R^2 \Delta r_{\parallel} - 1/3((r_{\parallel} + \Delta r_{\parallel}/2)^3 - (r_{\parallel} - \Delta r_{\parallel}/2)^3) \right), \tag{5}$$

with R half of the shortest side of the simulation box. In Fig. 1, we present the parallel pair correlation functions for the prolate nematic, oblate nematic, biaxial nematic, prolate uniaxial smectic, biaxial smectic of prolate symmetry and biaxial smectic of oblate symmetry.

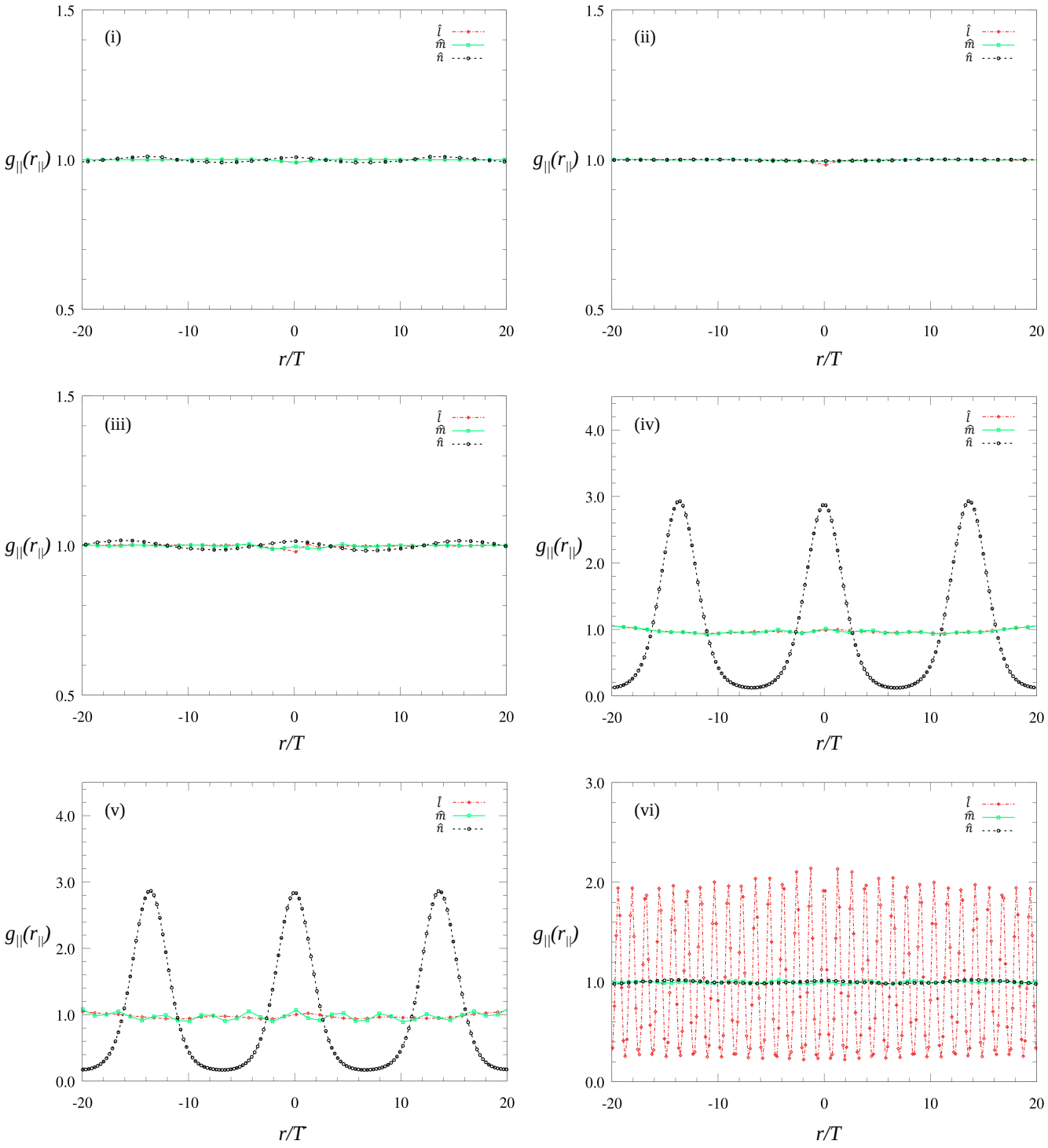

FIG. 1: Parallel pair distribution functions, $g_{\parallel}(r_{\parallel})$, along the nematic directors $\hat{\mathbf{l}}, \hat{\mathbf{m}}$ and $\hat{\mathbf{n}}$ of an (i) oblate nematic phase at $\sigma_L = 0.15$ and $\eta = 0.319$; (ii) prolate nematic phase at $\sigma_L = 0.10$ and $\eta = 0.342$; (iii) biaxial nematic phase at $\sigma_L = 0.25$ and $\eta = 0.487$; (iv) uniaxial smectic phase at $\sigma_L = 0.10$ and $\eta = 0.507$; (v) biaxial smectic phase with prolate symmetry at $\sigma_L = 0.10$; $\eta = 0.539$; and (vi) biaxial smectic phase with oblate symmetry at $\sigma_L = 0.18$ and $\eta = 0.546$.

III. SMECTIC LAYER THICKNESS

Tables IX to XIII show the average thickness of smectic layers, defined by $\tau^* = \tau/T$ of HBPs with $\sigma_L = 0.05$ to $\sigma_L = 0.20$.

TABLE IX: Reduced pressure, packing fraction and average thickness of smectic layers for HBPs of $\sigma_L = 0.05$.

P^*	η	τ^*
0.100	0.391	14.1
0.110	0.415	14.0
0.120	0.437	13.7
0.130	0.458	13.5
0.140	0.477	13.5
0.160	0.513	13.3
0.180	0.546	13.3
0.200	0.573	13.2

TABLE X: Reduced pressure, packing fraction and average thickness of smectic layers for HBPs of $\sigma_L = 0.10$.

P^*	η	τ^*
0.105	0.395	14.4
0.110	0.410	14.3
0.120	0.429	14.2
0.130	0.449	14.1
0.140	0.478	13.9
0.160	0.507	13.7
0.180	0.539	13.7
0.200	0.564	13.6

TABLE XI: Reduced pressure, packing fraction and average thickness of smectic layers for HBPs of $\sigma_L = 0.15$.

P^*	η	τ^*
0.120	0.429	14.7
0.130	0.449	14.6
0.140	0.478	14.5
0.150	0.507	14.5
0.160	0.539	14.4
0.180	0.564	14.3

TABLE XII: Reduced pressure, packing fraction and average thickness of smectic layers for HBPs of $\sigma_L = 0.18$.

P^*	η	τ^*
0.160	0.496	1.3
0.180	0.546	1.3
0.200	0.573	1.3

TABLE XIII: Reduced pressure, packing fraction and average thickness of smectic layers for HBPs of $\sigma_L = 0.20$.

P^*	η	τ^*
0.20	0.575	1.3

IV. FREE ENERGY CALCULATION

To gain an insight into the competition between prolate and oblate symmetries close to $\mathrm{I}-\mathrm{N_U}$ transition, we have compared the Helmholtz free energy of both $\mathrm{N_U^+}$ and $\mathrm{N_U^-}$ phases. To this end, we applied a fifth-virial Onsager-like theory developed in our work for monodisperse systems, where the Helmholtz free energy is obtained as a combination of an entropy of mixing-like term and a correction for many-body interactions via virial expansions [2]. We stress that we are using a theory developed for monodisperse systems to calculate the free energy of polydisperse systems and hence our results should only be taken as a qualitative estimation of the free energy difference between the $\mathrm{N_U^+}$ and $\mathrm{N_U^-}$ phases at a particular value of η. Interested readers are referred to Ref [2] for additional details. The free energy calculation of our polydisperse systems are performed in the context of free particle rotation and assumes that the dominant uniaxial order parameter in the prolate ($S_{2,L}$) and oblate ($S_{2,T}$) nematic phases have the same value. The four virial coefficients (B_2 to B_5) are obtained from the S_2 calculated by Monte Carlo simulations (reported in Table II to Table VIII). The phases we consider in this analysis are the $\mathrm{N_U}$ phases above the $\mathrm{I}-\mathrm{N_U}$ phase boundary for each polydispersity. For instance, at $\sigma_L = 0.05$, our simulation results indicate the formation of an $\mathrm{N_U}$ phase at $\eta = 0.310$ with dominant uniaxial order parameter $S_2 = 0.402$. These values of η and S_2 are used to obtain the corresponding virial coefficients and the entropy of mixing-like term for both $\mathrm{N_U^+}$ and $\mathrm{N_U^-}$ phases. In Fig. 2, the reduced free energy for $\mathrm{N_U^+}$ and $\mathrm{N_U^-}$ are shown for each size dispersity. For monodisperse systems, where $\sigma_L = 0.00$, the free energy of the $\mathrm{N_U^+}$ phase is lower than the $\mathrm{N_U^-}$ phase, suggesting that the system has a higher propensity to possess prolate symmetry, in agreement with Ref [2]. In polydisperse systems, the $\mathrm{N_U}$ phases are generally more likely to form $\mathrm{N_U^+}$ phases as well. However, the difference in free energy is such that relatively small density fluctuations, of the order of the thermal energy, might direct the systems to follow the oblate or prolate route, so determining their final symmetry. For $\sigma_L = 0.18$ and $\sigma_L = 0.25$, we find that these systems are more likely to form the $\mathrm{N_U^-}$ phase, a tendency that is consistent with our simulation results.

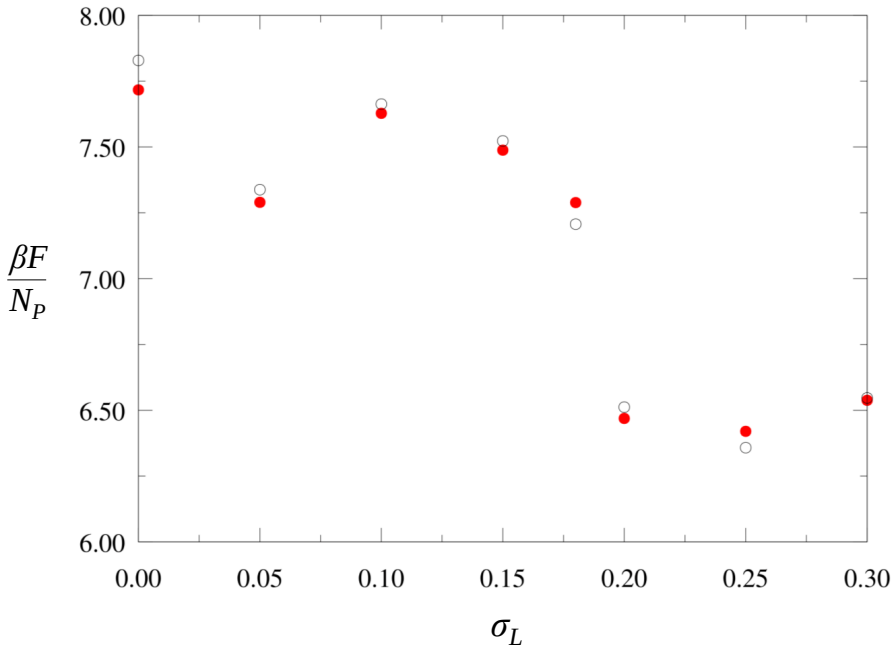

FIG. 2: Free energy per particle, plotted as a function of length polydispersity, σ_L. The parameter β is the inverse temperature. Each point corresponds to the first $\mathrm{N_U}$ phase that is observed above the I-N phase boundary. Solid and empty circles indicate, respectively, the free energy of prolate, $F^*_{N+} \equiv \beta F_{N+}/N_p$, and oblate, $F^*_{N-} \equiv \beta F_{N-}/N_p$ systems as obtained from theory.

With the same theory, the free energies F_{N+} and F_{N-} of $\mathrm{N_U}$ phases deep in the $\mathrm{N_U}$ region are also calculated. Tables XIV and XV show the estimated values of these free energies in monodisperse and polydisperse systems, respectively. Similar to what was observed for $\mathrm{N_U}$ phases just above the I-N phase boundary, the free energy of prolate and oblate phases deep in the $\mathrm{N_U}$ region are also very close to one another, suggesting an easy tendency for the systems to undergo director inversions with density fluctuations.

TABLE XIV: Reduced free energies of prolate, F^*_{N+}, and oblate, F_{N-}, uniaxial nematic phases deep in the N_U region of monodisperse systems. Free energies highlighted in bold indicate the most stable phase.

P^*	F^*_{N+}	F^*_{N-}
0.083	**7.717**	7.829
0.084	8.163	**8.149**
0.085	**8.221**	8.334
0.090	9.143	**8.996**

TABLE XV: Reduced free energies of prolate, F^*_{N+}, and oblate, F_{N-}, uniaxial nematic phases deep in the N_U region of polydisperse systems. Free energies highlighted in bold indicate the most stable phase.

P^*	σ_L													
	0.05		0.10		0.15		0.18		0.20		0.25		0.30	
	F^*_{N+}	F^*_{N-}	F^*_{N+}	F^*_{N-}	F^*_{N+}	F^*_{N-}	F^*_{N+}	F^*_{N-}	F^*_{N+}	F^*_{N-}	F^*_{N+}	F^*_{N-}	F^*_{N+}	F^*_{N-}
0.068	-	-	-	-	-	-	-	-	-	-	-	-	**6.597**	6.606
0.070	-	-	-	-	-	-	-	-	**6.469**	6.512	6.420	**6.358**	6.642	**6.568**
0.075	-	-	-	-	-	-	-	-	-	-	7.095	**7.079**	-	-
0.078	-	-	-	-	**7.488**	7.523	7.289	**7.207**	**-**	-	-	**-**	-	**-**
0.080	**7.290**	7.338	**7.628**	7.663	**7.484**	7.559	**7.759**	7.789	7.742	**7.660**	**7.713**	7.749	**7.660**	7.764
0.085	7.374	**7.229**	-	-	-	-	-	-	-	-	-	-	-	-
0.090	**8.787**	8.917	9.035	**8.963**	8.933	**8.862**	**8.694**	8.822	**8.745**	8.808	**8.630**	8.757	8.925	**8.839**
0.095	10.074	**9.936**	-	-	-	-	-	-	-	-	**9.327**	9.392	**9.271**	9.410
0.100	-	-	10.038	**9.876**	10.053	**10.023**	9.656	**9.480**	9.718	**9.700**	-	-	-	-
0.105	-	-	-	-	-	-	-	-	10.683	**10.603**	-	-	-	-
0.110	-	-	-	-	**11.112**	11.315	**10.919**	10.956	-	-	-	-	-	-
0.120	-	-	-	-	-	-	**12.289**	12.518	-	-	-	-	-	-

V. EQUATION OF STATE

In Fig. 3, we report the η *vs* P^* equation of state for systems of HBPs with polydispersity index $\sigma_L = (0.00, 0.30)$. The reduced pressure, P^*, is defined as $P^* \equiv \beta P T^3$, where β is the inverse temperature, P the pressure and T the particle thickness.

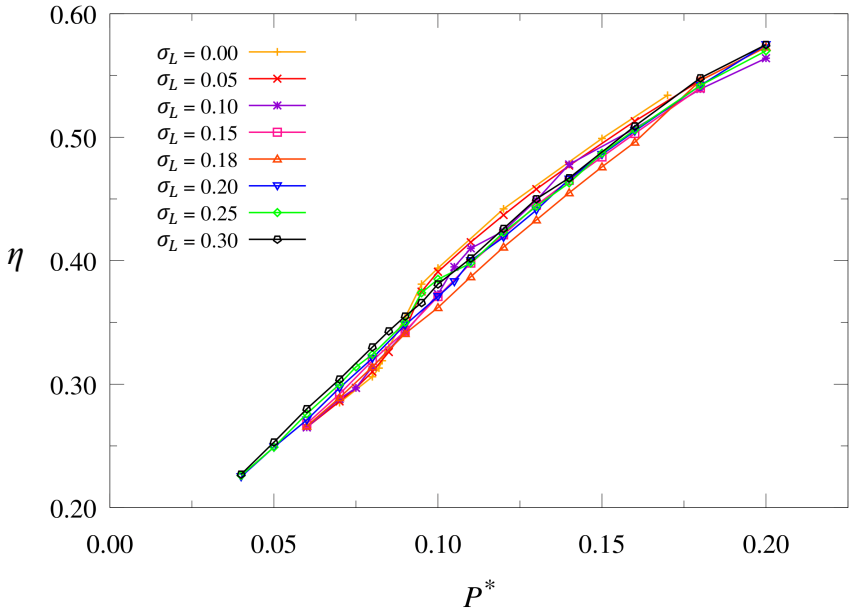

FIG. 3: Equation of state η *vs* P^* of HBPs at different values of σ_L. Solid lines are guides for the eyes.

[1] A. Cuetos, E. M. Rafael, D. Corbett, and A. Patti, Soft Matter, 2019, 15, 1922.
[2] A. Cuetos, M. Dennison, A. Masters and A. Patti, Soft Matter, 2017, 13, 4720.
[3] *Fases Fluidas Ordenadas mediante Modelos Moleculares Rígidos con Potenciales de Interacción Sencillos*. Alejandro Cuetos, Ed. Anavia. Sevilla, 2005, ISBN: 84-934302-0-X.